We are IntechOpen,
the world's leading publisher of Open Access books
Built by scientists, for scientists

4,800
Open access books available

122,000
International authors and editors

135M
Downloads

154
Countries delivered to

Our authors are among the

TOP 1%
most cited scientists

12.2%
Contributors from top 500 universities

CLARIVATE ANALYTICS
BOOK CITATION INDEX
INDEXED

WEB OF SCIENCE™

Selection of our books indexed in the Book Citation Index
in Web of Science™ Core Collection (BKCI)

Interested in publishing with us?
Contact book.department@intechopen.com

Numbers displayed above are based on latest data collected.
For more information visit www.intechopen.com

Phase Transition effect on the Parametric Instability of Liquid Crystals

Martin Hernández Contreras

Additional information is available at the end of the chapter

Abstract

We review advances in the last few years on the study of the Faraday instability onset on thermotropic liquid crystals of nematic and smectic A types under external magnetic fields which have been investigated with a linear stability theory. Especially, we show that thermal phase transition effects on nematics of finite thickness samples produce an enhanced response to the instability as a function of the frequency of Shaker's movement. The linear stability theory has successfully been used before to study dynamical processes on surfaces of complex fluids. Consequently, in Section 1, we show its extension to the study of the instability in the nematics, which set the theoretical framework for its further application to smectics or other anisotropic fluids such as lyotropic liquid crystals. We present the dispersion relationships of both liquids and its dependence on interfacial elastic parameters governing the surface elastic responses to external perturbations, to the sample size and their bulk viscosities. Finally, we point out the importance of following both experimental and theoretical analysis of various effects that needs to be incorporated into this model for the quantitative understanding of the hydrodynamics behavior of surface phenomena in liquid crystals.

Keywords: liquid crystals, parametric instability, surface hydrodynamics, phase transition, nonlinear waves, complex fluids

1. Introduction

The Faraday wave instability emerges as a macroscopic nonlinear behavior of the dynamics at interfaces of different liquids and vapor [1–22]. It appears when the vessel containing the liquid is vibrated vertically with a given acceleration until the quiescent equilibrium interface develops unstable surface waves. It has been observed in Newtonian fluids [6], but their most interesting realizations occur in complex fluids where their viscoelastic responses are present due to different time scales associated with the molecular relaxation processes [8, 16]. Therefore,

it is important to determine how the onset of the Faraday instability is determined by the underlying bulk fluid elasticity. The basic study of this phenomenon poses challenges to hydrodynamic and statistical theories that need to be adapted or developed to explain the onset of the instability. The description of the Faraday instability has recently motivated the advance of new experiments [23–26] and theoretical approaches for anisotropic fluids such as liquid crystals [27–40]. Also, it seems that its comprehensive experimental and theoretical investigation may have a major impact on the development of sensor technologies based on interfaces with biological or chemical components of practical interest. Absorbed molecules at the interface provide a surface coverage with absorbed molecular species that can present activity. Their impact on the instability has not well been understood yet. Liquid crystals remain as an ideal complex fluid where a controlled fine tuning of the cohesive energy of the absorbed molecules of interest and the nematogen's bulk average orientations imposed by surface treatment of their anchoring energy [41–46] can be experimentally reached. Reports on birefringent experiments on a lyotropic suspension of fd virus describe the effect of bulk microrheology on the surface wave [23]. The hysteresis of the wave amplitude under the harmonic external driving acceleration, and how the imposed perturbation shear lowers the viscosity for increasing driving impulse were observed. Such a rheological response of the liquid crystal led to a hydrodynamically induced transition from isotropic to nematic phase change, which produces the formation of patches at the deformed crest of the interface. In this chapter, we review recent work on the Faraday instability on thermotropic liquid crystals, and the effect that a thermal phase transition experienced by a nematic liquid crystal toward its isotropic state has on the instability onset. Thus, we review our understanding of thermal phase transitions that produce enhanced response on dynamical properties at the interface of thermotropic liquid crystals. The liquid crystal is subjected to vertical vibrations of the container which induce hydrodynamics instability on its surface. Temperature variations produce phase changes on liquid crystals [47]. We present our results on the liquid crystal phase change effect in the dynamics of the Faraday wave instability [39]. We focus our discussion on this coupled phenomenon on a hydrodynamic level of description based on the Navier-Stokes equation for the field velocity response of the liquid crystal. Our presentation incorporates the constitutive equation for taking into account properly the heat transfer into the liquid crystal which drives the phase transition. Also, the significant effects of various elastic parameters such as surface tension, bending modulus, and interfacial elasticity of the interface on the sustained wave are discussed. Further discussion shows how those elastic parameters determine the onset of the hydrodynamic instability through the critical acceleration of the surface wave, which is temperature dependent when the liquid crystal experiences a phase change. To set the theoretical framework, in Section 2 the phenomenological free energy of layers and surface deformations and its dependence on the elastic parameters are introduced. In Section 2.1, the hydrodynamic level of description of a model nematic liquid crystal is made. This section includes the mean field viscous shear stress tensor of the liquid crystal and the corresponding boundary conditions. In Section 2.2, we discuss the case of model nematic with nematogens aligned perpendicular to an external magnetic field but parallel to the surface. Such a model represents an isotropic liquid crystal case. We further present an analysis of the critical acceleration as a function of temperature variation from nematic up to the phase transition to the isotropic liquid crystal phase in Section 2.3. In Section 2.4, we analyze the dispersion relationship as a function of all elastic parameters

for a specific temperature. We then present in Section 2.5 the dispersion relation of an isotropic liquid. In Section 3, we discuss the occurrence of a parametric instability in smectic A liquids. In Sections 3.1 and 3.2, the finite thickness layer dispersion relationships for sustained Faraday surface waves in two configurations of the director on the magnetic field that orient the nematogens are provided. In Section 4, we discuss the experimental results in the literature on the phase transition effect on Faraday waves due to changes in particle concentration in a lyotropic liquid crystal of fd virus. In Section 5, a conclusion paragraph is provided. Finally, there is a list of the most relevant and updated list of references.

2. Thermotropic nematic liquid crystal layers

We consider a finite thickness layer of depth L of nematic fluid with its molecules been oriented parallel to the liquid-air interface in the X-axis direction by an external magnetic field H as shown in **Figure 1**.

The vector position giving the local elastic response of the interface has components $\zeta(x, y, t)$ and $\xi(x, y, t)$ to a normal and in-plane perturbations. Those deformation fields are determined by a surface tension γ and interfacial shear elasticity ε produced by adsorbed surfactants at the interface which lower the surface tension. Perturbations of the interface produce coupling of vertical and lateral deformation whose strength is given by a parameter λ. A splay module K determines the curvature distortion of the nematogen's layers deformation, and a compressibility modulus B yields its compression. The magnetic field orients the nematogens as they are characterized by a magnetic susceptibility χ_a. Thus, the elastic-free energy of layers distortion is given by [48]

$$F_{\text{bulk}} = \frac{1}{2}\int d^3 r \left\{ B(\partial_x u)^2 + K\left(\partial^2_y u + \partial^2_z u\right)^2 + \chi_a H^2 \left[\left(\partial_y u\right)^2 + \left(\partial_z u\right)^2 \right] \right\}. \tag{1}$$

whereas the interface elastic-free energy may be written approximately as [49]

$$F_{surface} = \frac{1}{2}\int d^2 r \left\{ \begin{array}{l} \gamma\left((\partial_x \zeta)^2 + (\partial_y \zeta)^2\right) + \varepsilon\left((\partial_x \xi)^2 + (\partial_y \xi)^2\right) + \kappa'\left(\partial^2_x \zeta + \partial^2_y \zeta\right)^2 \\ -2\lambda(\partial_x \xi)\left(\partial^2_x \zeta + \partial^2_y \zeta\right)^2 \end{array} \right\}. \tag{2}$$

The molecular field $u(x, y, z, t)$ takes into account the bulk elastic deformation of the stack of layers and which is caused by the acceleration, thermal fluctuations, and for smectics, also due to the movement (permeation) of molecules between layers $\dot{u} - v_x = \lambda_p h$, where λ_p, h is the permeation length and molecular field, respectively, $\partial_\beta := \partial/\partial_\beta$, $\beta = x, y, z$. If we consider the Faraday wave on a liquid crystal that supports a monolayer, then the surface elastic response is affected by surface tension, dilational, and coupling modulus as given in Eq. (2). Crilly et al. [50] have shown using photon correlation spectroscopy experiments that the thermotropic phase transition on monoglyceride monolayers that originate from the little molecular area fluctuations can be accurately detected. They found that two surface elastic moduli can explain the shear normal to the surface $\gamma = \gamma_0 - \pi + i\omega\gamma'$ and the other governs dilational distortion in
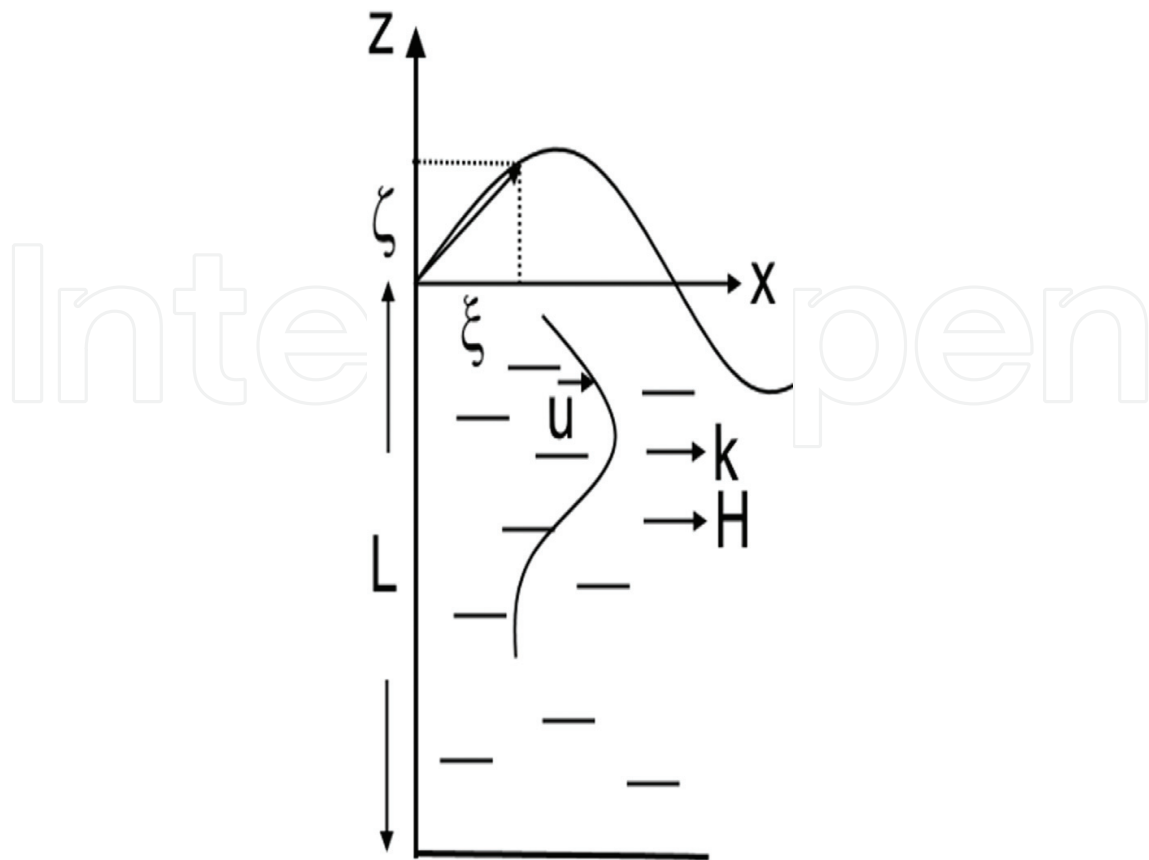
Figure 1. Interface of nematic liquid crystal layer of thickness L and air. A magnetic field **H** orients the nematogens parallel to the wave vector **k** which lies along the X-axis. Gravity modulation acts in the Z-axis direction. A vector position with components (ξ, ζ) designates the inplane and normal elastic deformation of the interface, respectively.

the interfacial plane $\varepsilon = \varepsilon_0 + i\omega\varepsilon'$. Both are complex quantities, with $i^2 = -1$ and γ', ε' viscous coefficients of a monolayer of surfactants with pressure π. γ_0, ε_0 are unperturbed values of elastic parameters without the monolayer. The imaginary parts are dissipative processes. However, Crilly et al. [50] showed that only the real parts of these moduli determine completely the thermotropic phase change of the surfactant monolayer, thus, our expression in Eq. (2) is valid to incorporate surface viscoelastic properties. The third elastic parameter λ that couples normal and tangential elasticity seems not to be detected experimenlly yet. The glycerol monooleate (GMO) monolayer has a phase transition temperature about $15.5°$**C** where a lipid undergos an all-trans state at low temperature to a gauche conformation of the lipid (pointing out the chain-melting transition) for temperatures greater than $15.5°$**C**. We note, however, that the liquid crystal methoxy benzylidine butyl aniline (MBBA) has a transition temperature of $45°$**C** [51]; therefore, one might expect a theory prediction for the effect of thermotropic phase changes of lipid monolayers on the Faraday waves to occur prior to the phase transition in the nematic-isotropic liquid. Such a study is possible to perform either experimentally and theoretically. From the experimental viewpoint, Crilly et al. [50] measured the elastic properties of the monolayer and provided results similar to those of **Figures 2** and **3** (see **Figure 1** of [50]), both well below and above the transition temperature as it is required in the modeling approach that is presented in this review. However, the determination of the
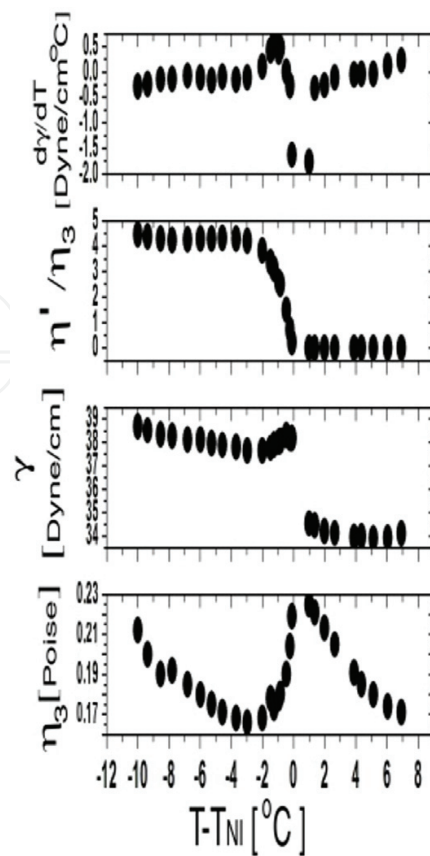
Figure 2. From bottom up are the interpolated values of viscosities η_3, surface tension γ, viscosity η'/η_3 of MBBA as a function of the nematic-isotropic phase transition temperature. These values were interpolated from the experimental studies of [54].

elastic properties of GOM monolayer and their variation as a function of temperature as in **Figures 1–3** of paper [50], when the monolayer is deposited on surfaces of liquid crystals, are still lacking, and their complete experimental measurement as a function of temperature would be quite valuable. Such experimental studies would pave the way for models which can be extended to understand thermotropic phase changes on monolayers and their impact on liquid crystal surface dynamics. Presently, one can resort to several useful models that study the surface hydrodynamics such as parametric instability, thermal capillary waves on polymer solutions and gels [13, 52], and coarse-grained effective field theories [27] and atomistic simulation techniques [37] and lattice hydrodynamics [17]. These methods have been demonstrated to provide a rich description of the effects of phase transition at interfaces of liquid crystals. From the experimental side, there is an accumulated knowledge of prototype systems that are now well characterized with tested experimental techniques. Those studies provide accurate information on static (elastic parameters [50, 53]). Also, the time-dependent properties (power spectrum of the intensity of scattered light) at interfaces of isotropic and simple liquids supporting surfactant monolayers [54] have been reported. Those studies need to be extended to include anisotropic liquids. An example of two such comprehensive experimental studies was performed by Langevin [54] in the 1970s where a series of systematic experiments on the variation of viscous and elastic parameters of some liquid crystals
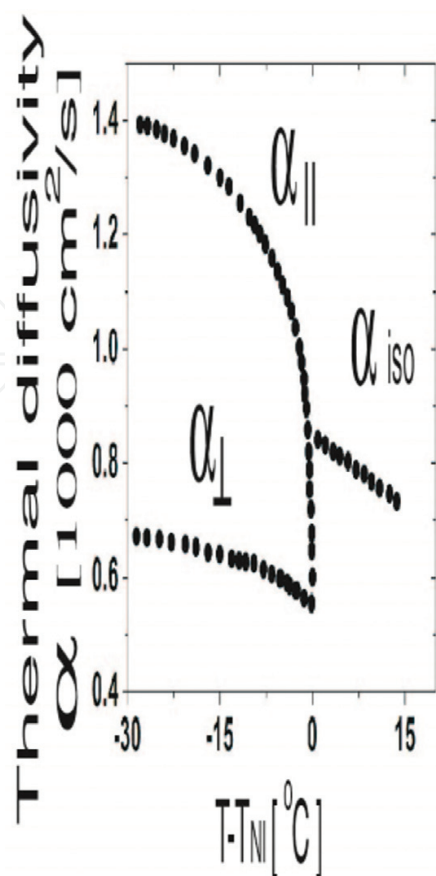
Figure 3. Interpolation of the entropy of deformation that contributes to Marangoni flow of nematogens during the thermal phase transition of MBBA from nematic to isotropic phase as a function of transition temperature. These values were interpolated from the experimental studies of [59].

experiencing thermotropic phase change were reported, and the thorough experiments by Earnshaw [55] on surfaces of water supporting monolayers of surfactants. These researches provided tabulated comprehensive data of the elastic parameters and viscous properties on bulk and in the plane of the interface in a wide range of temperatures and not only at a single specific temperature of interest. Our phenomenological description of the elastic behavior of the interface given in Eq. (2) relies on models developed for polymer solution surfaces with absorbed non-active surfactants [49]. They are simple models that do not incorporate the anchoring energy of nematogens on the liquid crystal side toward the lipid monolayer and its strength of variation. A more reliable model that takes into account surface elasticity and the modification of anchoring energy of nematogens due to absorption of lipids at surfaces was developed in [34–36], and the application of this method to study theoretically the main surface modes of thermal waves at surfactant-laden liquid-liquid crystal interfaces was made in [33]. In reference [33], it was predicted that the thermal wave has a dispersion law that involves energy dissipation through anisotropic coefficients due to compression of the surfactant layer. And a new relaxation mode of the director appears due to the boundary condition of anchoring at the interface in a perpendicular direction to the plane.

The experimental elucidation of thermotropic phase changes in monolayers of lipids deposited on top of liquid crystals and its impact on interface-laden of liquid crystals is an open topic to be investigated yet. A possible program for that task would involve the determination of the variation of the surface area of mono- or bilayers of surfactants like GMO which may be supported in isotropic, nematic, or smectic phases of liquid crystals. Moreover, the surface tension and dilational modulus versus temperature in an ample range around the critical temperature have been measured. Experimental techniques of photon correlation spectroscopy and surface quasielastic light scattering have been used in this context for isotropic fluids. Moreover, the entropy of formation of the film (see **Figure 2** in Ref. [50] for temperature gradient of surface tension), which is related to the Marangoni effect of diffusion of molecules in the surface, should be measured correspondingly. Such experiments might observe the phase transition in the film and also determine the surface viscosities ignored in our model of Eq. (2). It is expected that the viscosities will help in clarifying the nature of the monolayer phases [54–56]. A comprehensive experimental determination of the bulk Leslie viscosities of the most known liquid crystals in an ample interval of temperatures near their critical phase transition is scarce [53]. Their values can lead to the prediction of enhanced macroscopic hydrodynamic response on the parametric surface dynamics of liquid crystals [39, 40], or polymer melts [57]. A similar experimental program may be set up for studying lyotropic liquid crystals to determine the viscosities and elastic parameters as a function of temperature. Those thermodynamic parameters enter as inputs in models like the one developed in this section. As an alternative to experimental measurements of bulk and interfacial viscoelastic properties of liquid crystals, one can also resort to molecular dynamics simulation. This computational technique allows the determination of the bulk and surface elastic parameters for certain molecular models of liquid crystals where the nematogens are under pairwise forces of the Weeks-Chandler-Andersen type, and the particles of ellipsoidal shape constitute the colloidal suspensions. From the practical point of view, it is known that the viscoelastic behavior of films of surfactants has very practical consequences, for instance, the electrical properties of GOM films depend on the formation of pores arising from significant fluctuations in the area near the phase transition [37, 38].

2.1. Parallel magnetic field to wave vector and along the X-axis

In this section, we present the hydrodynamic description of the velocity field of the center of mass of an infinitesimal volume element containing nematogens and its corresponding boundary conditions on a fluid-air interface [39]. We consider a nematic layer in contact with air, which has an equilibrium interface that is located at position $z = 0$ and has a depth L and infinite lateral extension in order to avoid viscous boundary layer effects due to the wall of the container and also beneth the surface as it is shown in **Figure 1**. This model can be generalized to liquid-liquid interfaces that separate two phases of a liquid crystal. To ignore the finite size effect of the vessel, we assume that it has an infinite lateral extension. The fluid is subjected to vertical cosine-like vibration with an acceleration $g(t) = g - a \cos(\omega t)$, where a is the acceleration of the shaker in a reference frame fixed to the container. ω is the angular frequency of the oscillation and g being the gravitational acceleration. Because the director of

the nematogens remains fixed by the magnetic field, their time variation is neglected in the hydrodynamic equations. Under these conditions, a spatial ripple at the interface is generated which propagates symmetrically in the X- and Y-axis directions. Therefore, it is sufficient to consider that the surface wave propagates with wave vector k in the x-coordinate only and independently of coordinate y. The static magnetic field H keeps the director n=(1,0,0) of the nematogens in the X-axis direction oriented. Langevin calculated that thermal fluctuations produce periodic distortions of the nematic director with frequencies of strength $\omega_{undulation} = (Kk^2 + \chi_a H \cdot H)/\eta \approx 9.9$ Hz for MBBA nematic liquid with viscosity η. Both the frequency of the mechanical excitation and that of inertial effects $\omega_{inertia} = \eta/\rho L^2 = 10^6 \omega_{undulation}$ are larger than the elastic frequency of director variations. ρ is the density of the nematic. Thus, the nematic director dynamics is neglected in the hydrodynamic description of the generated surface wave. Therefore, the governing equation of the fluid velocity v about the quiescent state of rest is provided by the linearized Navier-Stokes equation which uses a reference frame that moves attached to the container [58]

$$\rho \frac{\partial V}{\partial t} = \nabla \cdot \sigma \tag{3}$$

The total stress tensor of the liquid $\sigma = -p\mathbf{I} + \sigma' + \sigma^r - \rho g(t)\widehat{\mathbf{e}}_z\widehat{\mathbf{e}}_z$ has dissipative contributions σ' due to the bulk viscous response and an elastic part σ^r given by the different elastic parameters in the free energy (Eq. (2)). Here, the unit vector $\widehat{\mathbf{e}}_z$ is directed along the Z-axis, and the hydrostatic fluid pressure is p. The unit matrix $\mathbf{I}_{\beta,\delta} = 1$ if $\beta = \delta$ and zero otherwise. For nematic liquids

$$\sigma'_{ij} = \eta' n_i n_j V_{l0} n_l n_0 + 2\eta_2 V_{ij} + 2(\eta_3 - \eta_2)(n_i n_l V_{lj} + n_j n_l V_{li}) \tag{4}$$

where the shear viscosities η_2, η_3, and η' are defined in terms of the Leslie coefficients as $\eta_3 = \frac{\alpha_2 + \alpha_5}{2} - \alpha_2 \gamma_2/(2\gamma_1)$, $\eta_3 = \frac{\alpha_4}{2}$, $\eta' = \alpha_1 + \gamma_2^2/\gamma_1$, where $\gamma_1 = \alpha_3 - \alpha_2$, and $\gamma_2 = \alpha_3 + \alpha_2$. The strain rate $V_{ij} = (\partial_i V_j + \partial_j V_i)/2$ has components $i, j, l, o = x, y, z$. For frequencies that are much less than the first sound frequency of the liquid, it holds the incompressible condition

$$\nabla \cdot V = 0. \tag{5}$$

In the experiment, a constant and vertical gradient of temperature that produces Marangoni flow with the rate of change of local temperature T variation given by the linearized heat diffusion equation [39] is applied from top to the bottom of the vessel

$$\frac{\partial T}{\partial t} = AV_z + \alpha(\partial_x^2 T + \partial_z^2 T) \tag{6}$$

where $A = -3^\circ$C/mm is the temperature gradient per unit length with the heating occurring from the air side. At the bottom solid wall $T = 0^\circ$C. The balance of the normal and tangential shear stresses at the interface $z = 0$ defines the boundary conditions to be

$$\sigma_{zz} = 0, \sigma_{xz} = 0, \sigma_{yz} = 0 \tag{7}$$

Normal interface displacements are balanced by the elastic force obtained from Eq. (2)

$$\sigma_{zz}^r = f_z = \gamma\left(\partial_x^2 + \partial_y^2\right)\zeta + \lambda\left(\partial_x^2 + \partial_y^2\right)\xi. \tag{8}$$

The tangential forces at the interface result from the Marangoni instability due to surface tension variation with temperature, and the in-plane elastic deformation which are obtained from Eq. (2) as

$$\sigma_{xz}^r = f_x = \frac{d\gamma}{dT}[\partial_x T - A\partial_x\zeta] - \varepsilon\left(\partial_x^2 + \partial_y^2\right)\xi + \lambda\left(\partial_x^2 + \partial_y^2\right)\zeta, \sigma_{yz}^r = 0. \tag{9}$$

In this last equation, elongational deformation ε and the coupling with normal deformation through the elastic parameter λ are included. This is the case when one needs to study interfaces that support mono- and bilayers of surface-active surfactants. Because the normal displacement is small compared with the wavelength, one can approximate the velocity field with the rate of surface deformations through the components of the vector that locates the interface positions as follows (see **Figure 1**):

$$\partial_t\zeta = V_z, \quad \partial_t\xi = V_x \text{ at } z = 0, \kappa\partial_z T = 0. \tag{10}$$

In the last equality, κ is the thermal conductivity of a thermally insolated surface with fixed flux. At the botton of the container $z = -L$, there is no slip of fluid

$$V = 0 \tag{11}$$

moreover, there is no penetration of the wall

$$\partial_z V_z = 0. \tag{12}$$

In the application that follows below, we do not consider the effect of the coefficients ε and λ and will be made zero. From the first two conditions of Eq. (7) and with help of Eq. (8), we obtain

$$\eta_3\left[\nabla_\perp^2 - \partial_z^2\right]V_z = \frac{d\gamma}{dT}\partial_x^2[T - A\zeta] \tag{13}$$

From the second identity of Eq. (7), and from Eq. (8) together with Eq. (9), we obtain

$$\left[\rho\partial_t - \eta_2\nabla^2\right]\nabla^2 V_z = (\eta_3 - \eta_2)\nabla^2\left[\partial_x\partial_z V_x - \partial_x^2 V_z\right] + \eta'\partial_x^2\partial_x\partial_z V_x. \tag{14}$$

Now taking the divergence with the gradient operator $\nabla_\perp := (\partial_x, \partial_y)$ of the Navier-Stokes (Eq. (3)) moreover, using the divergence of Eq. (4) yields

$$\nabla_\perp^2 p = \left[\rho\partial_t - \eta_2\nabla^2 - (\eta_3 - \eta_2)\partial_x^2\right]\partial_z V_z + (\eta_3 - \eta_2)\left[\nabla_\perp^2 + \nabla^2\right]\partial_x V_x + \eta'\partial_x^2\partial_x V_x \tag{15}$$

We now replace this expression in the z component of the total stress tensor σ and take its Fourier transform $\tilde{u} = \int d^2 r e^{i\mathbf{k}\cdot\mathbf{r}}u$, $i^2 = -1$ with the result (from now on, we will not use $\tilde{u}$ for any transformed function but just simply u)

$$\left[\partial_t + (v_3 + 2v_2)k^2 - v_2\partial_z^2\right]\partial_z V_z = -(v_3 - v_2)\left[-2ik^3 + ik\partial_z^2\right]V_x + v' ik^3 V_x - g(t)k^2\zeta - \frac{\gamma}{\rho}k^4\zeta. \quad (16)$$

As a consequence, the Fourier transformed form of Eq. (13) is

$$v_3\left[k^2 + \partial_z^2\right]V_z = \frac{k^2}{\rho}\frac{d\gamma}{dT}[T - A\zeta], \quad (17)$$

whereas Eq. (14) takes the form

$$\left[\partial_t - v_2\left(\partial_z^2 - k^2\right)\right]\left(\partial_z^2 - k^2\right)V_z = (v_3 - v_2)\left(-\partial_z^2 + k^2\right)\left[ik\partial_z V_x + k^2 V_z\right] + v' ik^3\partial_z V_x, \quad (18)$$

With $v_j:=\frac{\eta_j}{\rho}, j = 2, 3, v':=\eta'/\rho$. Similarly, Eq. (6) becomes

$$\frac{\partial T}{\partial t} = A V_z + \alpha\left(\partial_z^2 T - k^2 T\right), \quad (19)$$

The acceleration $g(t)$ is a function with period $2\pi/\omega$, and according to Floquet theory the solution of Eqs. (5) and (16)–(19) is the superposition $\zeta(t) = \sum_{n=-\infty}^{\infty} \zeta_n \exp\left(\mu_n t\right)$ [6]

where the modes $\mu_n = s + i(n + \alpha_r)\omega$. The quantities ζ_n, s, α_r are real numbers. There are two types of waves Harmonic with frequency equaling the external forcing frequency and determined by $\alpha_r = 0$, with ζ_n equaling its complex conjugate and subharmonic with $\alpha_r = 1/2$, with $\zeta_n = \zeta_{n-1}^*$. The velocity V_z also has a similar Floquet expansion that is substituted in Eqs. (5) and (18) providing the equation for each component of the velocity amplitude V_{zn}

$$\left[\partial_z^4 + b_n\partial_z^2 + c_n\right]V_{zn}(z) = 0, \quad (20)$$

where $b_n = -\left[\frac{\mu_n}{v_3} + k^3\left(2 + \frac{v'}{v_3}\right)\right], c_n = k^2\left[\frac{\mu_n}{v_3} + k^2\right]$. A trial solution of Eq. (20) in the form $v_{zn}(z)$ $\sim e^{m(k)z}, C = m^2$ simplifies Eq. (20) to $C^2 + b_n C + c_n = 0$. We denote the two possible modes $C_j := m_j^2, j = 1, 2$ which lead to the solution of Eq. (20) in the form

$$V_{zn}(z) = P_n \cosh(zm_1) + Q_n \sinh(zm_1) + R_n \cosh(zm_2) + S_n \sinh(zm_2). \quad (21)$$

The coefficients P_n, Q_n, R_n, S_n in this solution are derived by the substitution of Eq. (21) in Eqs. (10)–(12) (we recall $\xi = \lambda = 0$ here). Finally, the use of Eq. (21) in Eq. (16) yields the surface amplitude of deformation ζ_n

$$M_n\zeta_n = a(\zeta_{n-1} + \zeta_{n+1}) \quad (22)$$

with

$$M_n = \frac{2}{k}\left\{\begin{array}{l} w_0^2 + \frac{m_1}{k}\left[\mu_n + k^2\left(3v_3 + v'\right) - v_3 m_1^2\right]\frac{Q_n}{\zeta_n} + \\ + \frac{m_2}{k}\left[\mu_n + k^2\left(3v_3 + v'\right) - v_3 m_2^2\right]\frac{S_n}{\zeta_n} \end{array}\right\} \equiv \frac{2}{k}D_n, \quad (23)$$

moreover, the capillary frequency $w_0^2 := gk + \frac{\gamma k^3}{\rho}$. The coefficients are

$$Q_n = \frac{\zeta_n \mu_n A_1}{\left(m_1^2 - m_2^2\right)\left(1 + \frac{k^2 \alpha}{\mu_n}\right)de}$$

$$A_1 = -m_2\left(k^2 + m_1^2\right) - m_2\left[k^4\left(\frac{A}{\mu_n \eta_3}\frac{d\gamma}{dT} + 1\right) + k^2 m_1^2\right]\frac{\alpha}{\mu_n} +$$

$$\left\{k^2 + m_2^2 + \left[k^4\left(\frac{A}{\mu_n \eta_3}\frac{d\gamma}{dT} + 1\right) + k^2 m_2^2\right]\frac{\alpha}{\mu_n}\right\}.$$

$$(m_2 \cosh(Lm_1)\cosh(Lm_2) - m_1 \sinh(Lm_1)\sinh(Lm_2)),$$

$$S_n = \frac{\zeta_n \mu_n B_1}{\left(m_1^2 - m_2^2\right)\left(1 + \frac{k^2 \alpha}{\mu_n}\right)de}$$

$$de := -m_2\cosh(Lm_2)\sinh(Lm_1) + m_1\cosh(Lm_1)\sinh(Lm_2),$$

$$B_1 = -m_1\left(k^2 + m_2^2\right) - m_1\left[k^4\left(\frac{A}{\mu_n \eta_3}\frac{d\gamma}{dT} + 1\right) + k^2 m_2^2\right]\frac{\alpha}{\mu_n} +$$

$$\left\{k^2 + m_1^2 + \left[k^4\left(\frac{A}{\mu_n \eta_3}\frac{d\gamma}{dT} + 1\right) + k^2 m_1^2\right]\frac{\alpha}{\mu_n}\right\}.$$

$$(m_1 \cosh(Lm_1)\cosh(Lm_2) - m_2 \sinh(Lm_1)\sinh(Lm_2)),$$

$$P_n = -\frac{\zeta_n \mu_n}{m_1^2 - m_2^2}\left[k^2 + m_2^2 + k^4\frac{A}{\mu_n \eta_3}\frac{d\gamma}{dT}\frac{(\alpha/\mu_n)}{\left(1 + k^2\frac{\alpha}{\mu_n}\right)}\right],$$

$$R_n = \frac{\zeta_n \mu_n}{m_1^2 - m_2^2}\left[k^2 + m_1^2 + k^4\frac{A}{\mu_n \eta_3}\frac{d\gamma}{dT}\frac{(\alpha/\mu_n)}{\left(1 + k^2\frac{\alpha}{\mu_n}\right)}\right],$$

(24)

Eq. (22) is the first of our most significant results. It permits the calculation of the wave amplitude modes ζ_n as dictated by the viscoelastic properties of the nematic liquid and the hydrodynamic fluid velocity. It does not depend on adjustable free parameters and includes the Marangoni number $Ma = (A/\mu_n \eta_3)d\gamma/dT$ that takes into account the thermal instability induced by the heating process applied to the nematic layer. All the material parameters that appear in Eq. (22) have already been reported by the experimental work of other authors [58] and that we are going to use further in the subsequent text. In contrast for a system of semi-infinite thickness, we obtained

$$M_n^\infty = \frac{2}{k}\left(w_0^2 - \frac{\mu_n}{k(m_1 + m_2)\left(1 + k^2\frac{\alpha}{\mu_n}\right)}\left\{\begin{array}{c}\left[\mu_n + k^2\left(3v_3 + v'\right)\right]\left(k^2 - m_1 m_2\right)\\ -v_3 k^2\left(m_1^2 + m_2^2 + m_1 m_2\right) - v_3 m_1^2 m_2^2\\ +\frac{\alpha}{(m_1 - m_2)^2}\left[\begin{array}{c}A_2\left(m_1 m_2 + v_3 m_1 m_2^3 + B_3 m_2^2 - v_3 m_2^4\right)\\ +B_2\left(m_1 m_2 + v_3 m_2 m_1^3 + B_3 m_1^2 - v_3 m_1^4\right)\end{array}\right]\end{array}\right\}\right)$$

(25)

$$\equiv \frac{2}{k}D_n^\infty\left(k, \mu_n = s + i(\alpha_r + n)\omega\right),$$

where the coefficients

$$A_2 = k^4\left(\frac{A}{\mu_n \eta_3}\frac{d\gamma}{dT} + 1\right) + k^2 m_1^2, \quad B_2 = k^4\left(\frac{A}{\mu_n \eta_3}\frac{d\gamma}{dT} + 1\right) + k^2 m_2^2 \text{ and } B_3 = \mu_n + (3\nu_3 + \nu')k^2.$$

2.2. Magnetic field in the Y-axis direction with wave vector along the X-axis

In this section, we consider a nematic liquid layer of thickness L with the average director of nematogens $\mathbf{n}=(0,1,0)$ oriented in the Y-axis direction by the magnetic field and the wave propagates with wave number k in the X-axis. Thus, there is no coupling of the director with the flux. The hydrodynamic Navier-Stokes equation is the same as an isotropic liquid with a single viscosity $\eta := \eta_3 = \eta_2$. The components of the viscous stress tensor in Eq. (4) now read [53]

$$\sigma'_{xx} = 2\eta \partial_x V_x, \quad \sigma'_{zz} = 2\eta \partial_z V_z, \quad \sigma'_{zx} = \eta(\partial_x V_z + \partial_z V_x). \tag{26}$$

Moreover, the forces normal to the interface and in the plane are, respectively, the same as in Eqs. (8)–(9) of Section 4. The boundary conditions are the same as in Eqs. (10)–(12), and the heat diffusion equation (Eq. (13)) is still valid. Consequently, the same method of section **a** results in the following eigenvalue equation for the mode amplitude of the wave:

$$M_n^i \zeta_n = a(\zeta_{n-1} + \zeta_{n+1}), \tag{27}$$

with

$$M_n^i = \frac{2}{k}\left\{w_0^2 + \nu(q_n^2 + k^2)\frac{Q_n^i}{\zeta_n}\right\} + 4\nu q_n \frac{S_n^i}{\zeta_n}, \tag{28}$$

and

$$Q_n^i = \zeta_n \begin{pmatrix} \nu q_n k^2 \left\{-2\left(1 + k^2\frac{\alpha}{\mu_n}\right) + \frac{A}{\nu\eta}\frac{d\gamma}{dT}\frac{1}{k^2 - q_n^2}\left[1 - q_n^2\frac{\nu}{\mu_n} + (\nu + \alpha)\frac{k^2}{\mu_n}\right]\right\} + \\ \nu\left\{-(k^2 + q_n^2)\left(1 + k^2\frac{\alpha}{\mu_n}\right) + \frac{A}{\nu\eta}\frac{d\gamma}{dT}\frac{k^2}{k^2 - q_n^2}\left[1 - q_n^2\frac{\nu}{\mu_n} + (\nu + \alpha)\frac{k^2}{\mu_n}\right]\right\} \\ \times \left[-q_n\cosh(kL)\cosh(q_nL) + k\sinh(kL)\sinh(q_nL)\right] \end{pmatrix}$$
$$\times \left\{\left(1 + k^2\frac{\alpha}{\mu_n}\right)\left[q_n\sinh(kL)\cosh(q_nL) - k\cosh(kL)\sinh(q_nL)\right]\right\}^{-1} \tag{29}$$

2.3. Thermal phase transition effect on surface dynamics

In this section, we study the critical acceleration, and wave number of the Faraday wave at the interface of nematic liquid crystal and air as a function of temperature. We use the real material parameters reported in the literature of nematic methoxy benzylidene butyl aniline liquid crystal that experiences a thermal nematic-isotropic phase transition [58]. We now explain how we calculated the wave properties just mentioned. These properties a_c, k_c need to be determined in the nematic phase and then in the isotropic phase of the liquid. Notice that the

critical parameters are obtained in separate plots of the driving acceleration a for the onset of Faraday waves versus wave number. The lowest value of $a = a_c$ in the lower branch in that plot for a given k yields their critical values, so we need to first see this plot, the so-called instability tongue because of its shape, to know what it is the corresponding minimum value of a and associated wave number. One of such plots is given in **Figure 4** of the neutral stability curve.

This picture was obtained using Eq. (27) for a semi-infinite medium of nematic and temperature of $T_{NI} - T = 3^\circ$C from the nematic-isotropic transition temperature and the experimental data for MBBA $\eta_3 = 0.0163$ Pa s, $\gamma = 0.03853$ N/m, $\rho = 1.03881 \times 10^3$ kg/m^3 [58]. The main wave sustained by the interface is of subharmonic type.

For the pure nematic state, we first solved numerically Eqs. (22)–(24) with $s = 0$, $\alpha_r = 1/2$ for $n = 22$ modes using the real materials data of the nematic MBBA obtained from interpolations of the experimental data which are provided in **Figures 2** [58] and 3 [59]. Experiments with laser light scattering from the interface of MBBA performed by Langevin [54, 58] show that the nematic state has two viscosities η', η_3, the surface tension α and the interface structural entropy $d\gamma/dT$ as the only necessary data to characterize fully the phase transition. MBBA has the critical temperature of $T_c \approx 45^\circ$C, and above this temperature the anisotropy of the viscosity disappears. This was confirmed experimentally by Langevin who found that in the isotropic state of the liquid the intensity of scattered light is well characterized by a single bulk viscosity $\eta = \eta_3 = \eta'$ and the same elastic parameters above. In both cases, the density of the liquid crystal was the same and equal to the constant value $\rho = 1.03881 \times 10^{-3}$ kg/m^3 as required by the
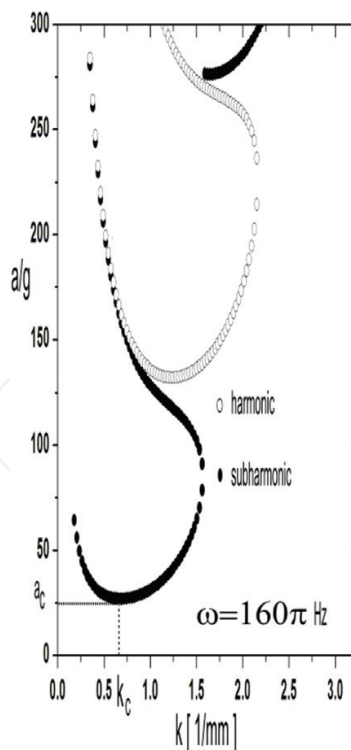

Figure 4. Neutral stability curve of Faraday waves of subharmonic type for a semi-infinite layer of nematic in contact with an air interface. The use was made of the real material parameters of MBBA $\eta_3 = 0.0163$ Pa s, $\gamma = 0.03853$ N/m, $\rho = 1.03881 \times 10^3$ kg/m^3, and temperature $T_{NI} - T = 3^\circ$C from the phase transition.

incompressibility condition (Eq. (5)). We used a liquid layer of thickness $L = 4.5$ mm. Thus, for the isotropic phase we used the hydrodynamic equations which are similar to those of a simple liquid derived in this section. The critical parameters were numerically calculated from Eqs. (27)–(29) for the isotropic branch. The result of such a procedure is depicted in **Figure 5**.

Figure 5 shows the transition of the main sustained waves which are of subharmonic type, from low up to high temperatures across the critical temperature. One can observe that there is a significant variation of (a_c, k_c) due to their discontinuous behavior at the critical temperature of phase transition. **Figure 5a** and **b** depict k_c, and **Figure 5c** yields a_c, versus the nematic-isotropic transition temperature $T - T_c$ at two values of the external frequency ω. For $\omega = 20\pi$ Hz, the plots of **Figure 5a** and **c** with symbol O correspond to the inclusion of Marangoni flow. For a higher frequency $\omega = 40\pi$ Hz we used symbol ● in **Figure 5b** and **c** and Marangoni flow is included too. However, in **Figure 5** the plots with symbol ★ do not include Marangoni flow. We used the viscosities and surface tension in all the ranges of temperature variations as shown in **Figures 2** and **3**. When the Marangoni number is included $Ma = (A/\mu_n \eta_3)d\gamma/dT$ in Eqs. (22)–(24) and (27)–(29), the critical acceleration and wave number (a_c, k_c) roughly coincide with their values when $Ma = 0$ is neglected. The same results are obtained if the anistotropy of the thermal diffusivity is taken as either $\alpha_{\parallel}$ or $\alpha_{\perp}$; therefore in the plot of **Figure 5** only $\alpha_{\parallel}$ for the nematic side and α_{iso} for the isotropic branch are used. On the other hand, from **Figures 2** and **3** we can observe that the vertically applied temperature gradient of $A = -3°$C/mm on top of MBBA produces major changes in the magnitude of viscosities, surface tension, and on thermal diffusivity. However, the single parameter, the gradient of surface tension $\frac{d\gamma}{dT}$, which is related to Marangoni flow, does not affect the Faraday wave. This phenomenon occurs for instance at $\omega = 40$Hz in **Figure 5**. We note from **Figure 5** that (a_c, k_c) display the same discontinuous behavior as the viscous and elastic parameters do across the thermal phase transition temperature. However, a different mechanism for discontinuity of these critical parameters was measured experimentally by Huber et al. [57] during the surface freezing of a polymer monolayer made of tretraconazole melt. They found that a decrease of temperature leads to the formation of a monolayer at the interface of polymer-air that changed the surface tension but without an observable quantitative change of bulk viscosity. As a consequence, a high flow velocity gradient close to the surface at a characteristic temperature during the cooling down process from the high temperature regime is produced. Such an effect was accurately confirmed with a Faraday wave calculation by those authors and it is similar to our results here. We note that an exact match of the experimentally measured power spectrum of scattered light by thermal fluctuations of the nematic-air interface with a theoretical calculation ignoring Marangoni flow and for constant temperature suggests that a monolayer of nematogens does not form at the interface of MBBA. Unlike the MBBA liquid, the critical parameters of the Faraday instability at the interface of the liquid-vapor of CO_2 [6] do not display discontinuous behavior as in the liquid crystal study.

2.4. Dispersion relation of an MBBA liquid layer with the inclusion of Marangoni flow

In **Figure 6**, the dispersion relation of the real MBBA (**Figure 6a**) together with an ideal model of a nematic (**Figure 6b** and **c**) as calculated from Eqs. (22)–(24). The real MBBA liquid
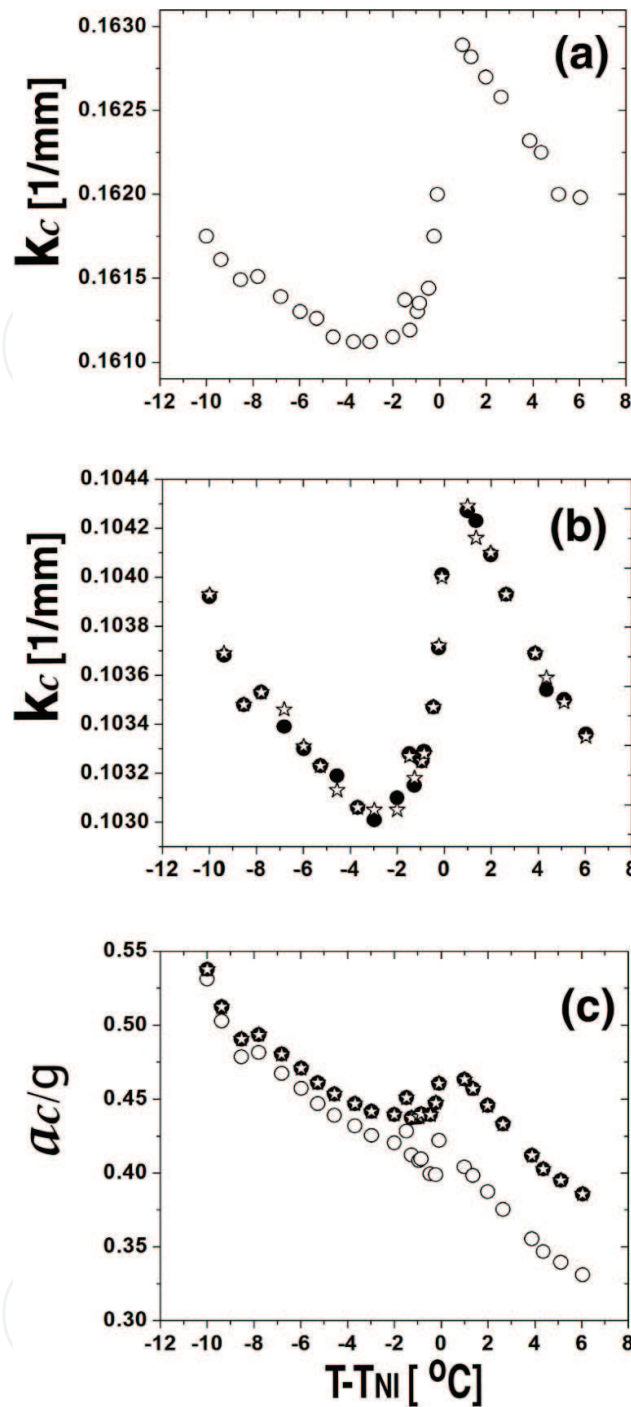
Figure 5. Calculated critical parameters of the Faraday wave during a thermal phase transition of nematic MBBA. In **Figure 5**, the critical wave number k_c (5a, 5b) and acceleration a_c (5c) as a function of the transition temperature are plotted. Two cases of frequency of excitation were used, $\omega = 20\pi$ Hz with symbol O, (5a, 5c), $\omega = 40\pi$ Hz symbol ● and white stars (5b, 5c). The nematic layer depth is $L = 4.5$ mm. Symbols O and ● include Marangoni flow, and it is neglected in the plot with a star symbol. The material parameters used across the thermal phase transition are those given in **Figures 2** and **3**.

(**Figure 6a**) presents a minimum of $a_c \approx 0.455$ g at oscillaton frequency $\omega = 55\pi$ Hz for a layer thickness of $L = 4.5$ mm. In this picture, the Marangoni flow was included, whereas the ideal model of nematic has a higher viscosity $\eta_3 = 0.163$ Pa than the real one, and its thickness is
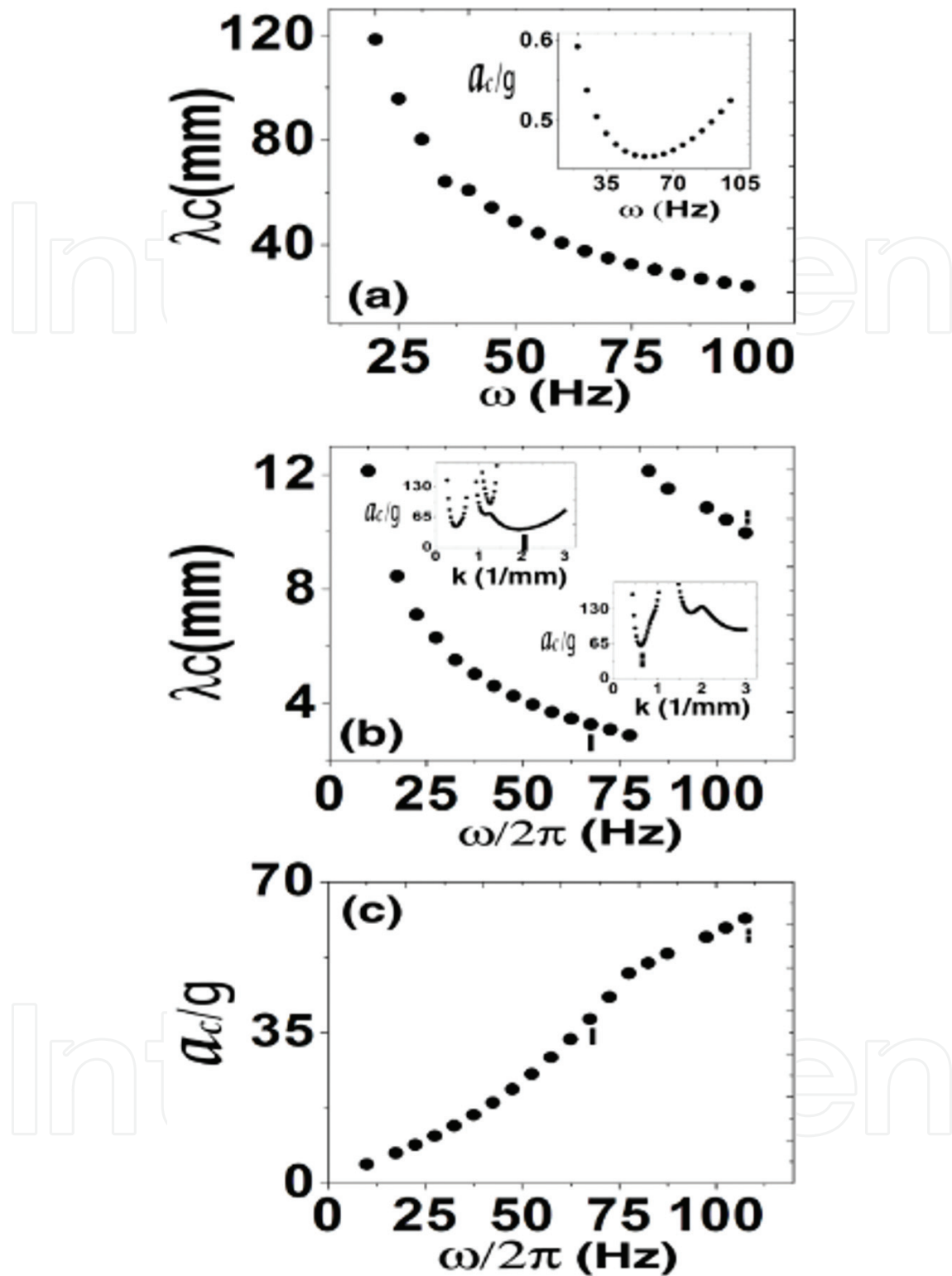
Figure 6. Dispersion relation of subharmonic waves of nematic MBBA at the fixed transition temperature $T_{NI} - T = 3°$C for layer thickness of $L = 4.5$ mm (6a) and $L = 2.5$mm for (6b, 6c). Inset in **Figure 6a** depicts the critical acceleration calculated using the real parameters of MBBA and inclusion of Marangoni flow was made. Pictures in **Figure 6b** and **c** are for a model of nematic with 10 times the viscosity of the real nematic and neglect Marangoni flow and its critical acceleration is given in 6c. The left and right vertical lines in the insets of panels b and c depict the critical accelerations $\frac{a_c}{g} = 38.12, 51.13$ which occur at wave vectors $k_c = 1.9284, 0.6312$ mm^{-1} and frequencies $\omega = 135\pi, 215\pi$ Hz, respectively.
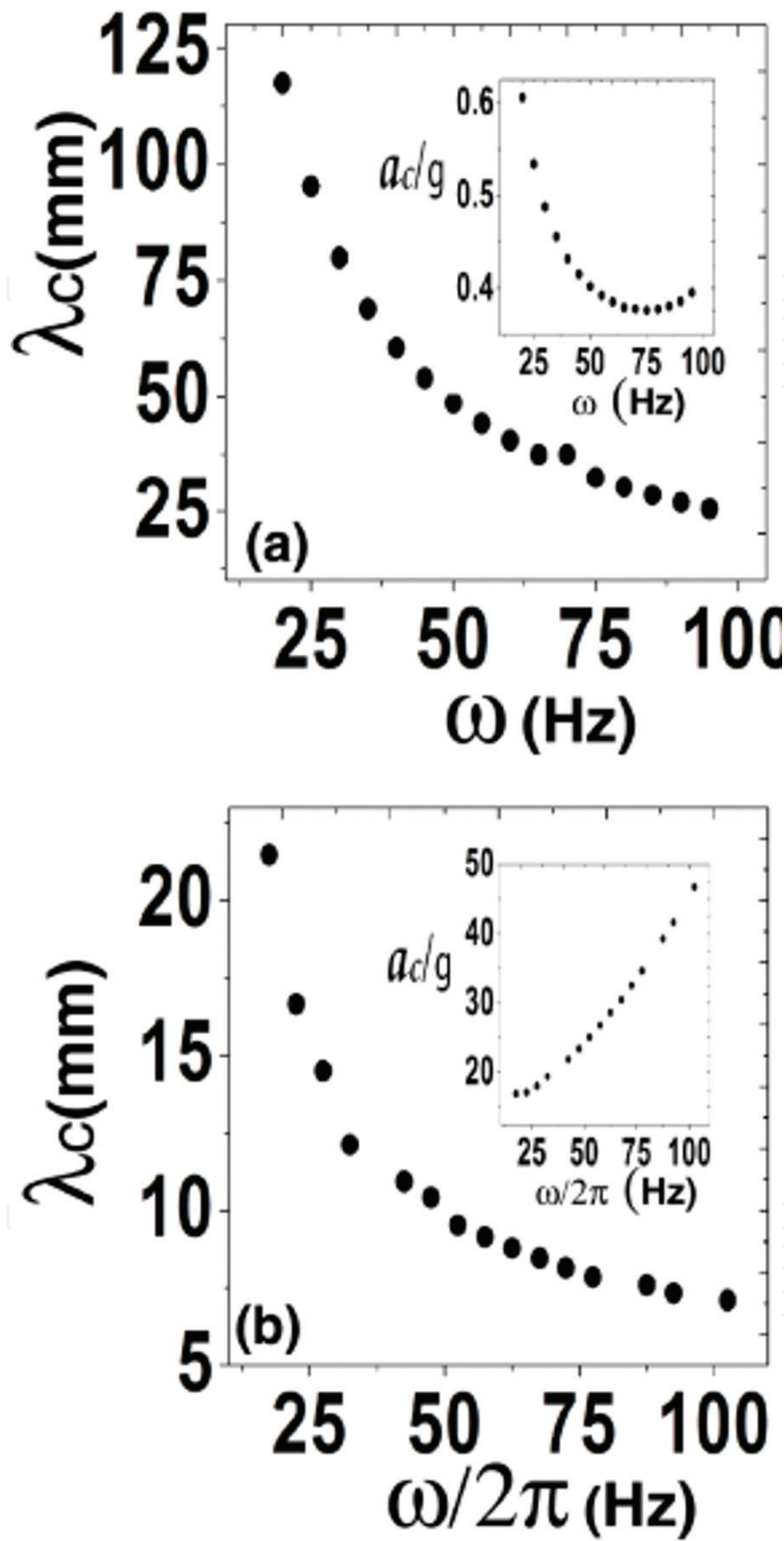
Figure 7. Dispersion relation of subharmonic waves of the isotropic nematic for low nematic depths $L=4.5, 2.5$ mm, **Figure 7a** and **b**, respectively. Other parameters are as in **Figure 6**. **Figure 7a** includes Marangoni number and uses real data of MBBA, whereas **Figure 7b** is for a model nematic with 10 times the real viscosity with no Marangoni flux. The insets correspond to the critical acceleration versus frequency.

almost half the size of the real MBBA $L = 2.5$ mm without Marangoni instability. The ideal model shows a monotonously increasing critical acceleration versus frequency (**Figure 6b** and **c**). A similar minimum value of a_c was detected in silicon oil and water system. From **Figure 6b** and **c**, it can be seen that the harmonic type wave length λ_c versus frequency shows a bifurcation. First, λ_c decreases continuously as the frequency starts growing until a value $\omega \approx 165\pi$ Hz is reached and suddenly the wave length makes a jump to a new value of the same magnitude $\lambda_c = 12.12$ mm; it has at the starting value of the stimulus excitation $\omega \approx 20\pi$ Hz. The inset in **Figure 6b** shows this transition in a regime of critical acceleration depicted with the small vertical lines. The discontinuities in wave length have been documented also to appear in viscoelastic fluids, in Newtonian liquids, and for silicon water oil systems.

2.5. Dispersion relation of isotropic liquid crystal layer with the inclusion of Marangoni flow

In this case, the dispersion relation is calculated from Eqs. (27)–(29). **Figure 7** presents the dispersion relation, whereas the insets depict the curve of the critical acceleration as a function of frequency for two systems; one with a layer thickness of $L = 4.5$ mm, **Figure 7a** that includes Marangoni flow, and the second one for $L = 2.5$ mm with $Ma = 0$ as shown in **Figure 7b**. The same pattern of behavior as in **Figure 6** is obtained.

3. Thermotropic smectic A liquid crystal layers

3.1. Smectic order parameter, wave vector, and magnetic field directed along the X-axis direction

In this section, we discuss the Faraday instability in smectic A liquid crystal layers [40]. We consider a smectic liquid crystal of average thickness L and infinite lateral extension in contact with a vapor. The nematogens are oriented by an external magnetic field in the X-axis as depicted in **Figure 8**.

The stack of layers deformation is given by Eq. (1), whereas the elastic response of the interface is given by Eq. (2). The governing hydrodynamic equations of the velocity, viscous stress tensor, and the boundary conditions were reported in Refs. [40, 53]. Following their use and with the help of the methods of Section 2, we derived the following recursive equation of the amplitude of deformation ζ_n:

$$M_n \zeta_n = a(\zeta_{n-1} + \zeta_{n+1}) \tag{30}$$

$$M_n = \frac{2}{k} \left\{ w_0^2 + \left\{ \frac{\left[Bk^2 + KS_1^2 + Kk^2 S_1 + \chi_a H^2 S_1 \right]}{\rho} + \left[\mu_n + \lambda_p Bk^2 + \lambda_p \left(KS_1^2 - \chi_a H^2 S_1 \right) \right] \left[\mu_n + k^2 (3\nu_3 + \nu') - \nu_3 S_1 \right] \right\} \frac{(A_1 + B_1)}{i\zeta_n} \right\},$$
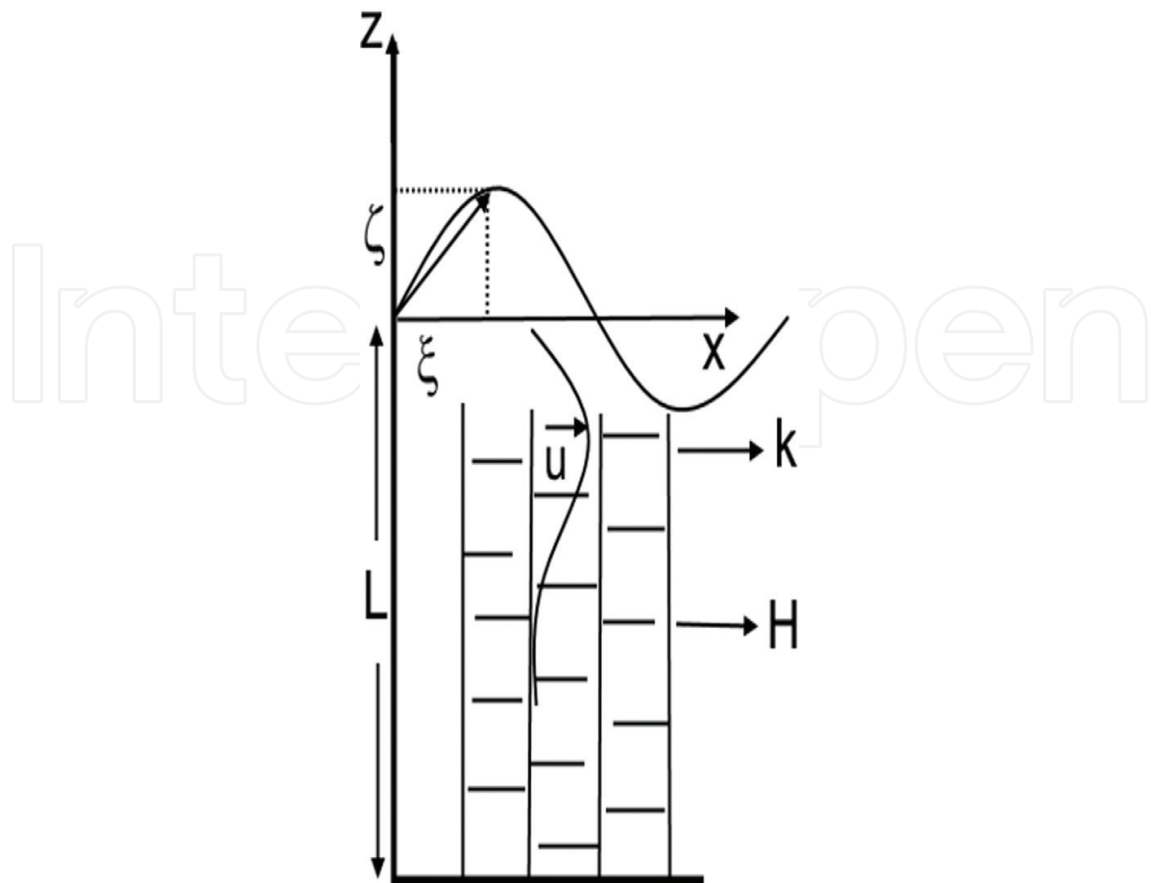
where

Figure 8. Model of the deformation of a smectic A liquid crystal layer of thickness L due to the external perturbation. The liquid crystal has a free interface with air. The nematogens are oriented by a magnetic field **H** in the X-axis direction and parallel to the interface surface. The velocity flow given by the wave vector k is parallel to the external field.

$$A_1 = \frac{\zeta_n i e^{L\sqrt{S_1}}}{2kR_n\sqrt{S_1}}\left(-1 + \coth(L\sqrt{S_1})\right)[\mu_n S_1 + k^2(-1 + e^{L\sqrt{S_1}})R_n]$$

$$B_1 = \frac{\zeta_n i}{kR_n\sqrt{S_1}(-1 + e^{L\sqrt{S_1}})}[\mu_n S_1 e^{L\sqrt{S_1}} - k^2(-1 + e^{L\sqrt{S_1}})R_n]$$

$$R_n = \lambda_p BK^2 + \lambda_p KS_1^2 - \lambda_p \chi_a H^2 S_1 + \mu_{n'}, S_1 = k^2 d_n/c_{n'}$$

$$c_n = \frac{\mu^2{}_n}{\lambda_p K\nu_3} + k^2\left(\frac{\mu_n}{\lambda_1^2\nu_3} + \frac{\mu_n}{\xi_H^2\nu_3} + \frac{2\mu_n}{\lambda_p K} + \frac{\nu'\mu_n}{\lambda_p K\nu_3} + \frac{\kappa_s{}^2}{\lambda_1^2}\right) + k^4\left(\frac{1}{\xi_H^2} + \frac{2}{\lambda_1^2} + \frac{\nu'}{\nu_3\lambda_1^2}\right)$$

$$d_n = \frac{\mu^2{}_n}{\lambda_p K\nu_3} + k^2\left(\frac{\mu_n}{\lambda_1^2\nu_3} + \frac{\mu_n}{\lambda_p K}\right) + \frac{k^4}{\lambda_1^2}, \xi_H = \sqrt{K/\chi_a}/H, \lambda_1 = \sqrt{K/B},$$

$$\lambda_p = \frac{1}{\rho\nu_3\kappa_s{}^2}, \nu' = \frac{\eta'}{\rho}, \kappa_s \approx 100\,\overset{o}{A}.$$

In this eigenvalue equation, we ignored the elongational elasticity and coupling between in-plane and normal elastic deformations. A plot of the Faraday stability curve is given in **Figure 9**
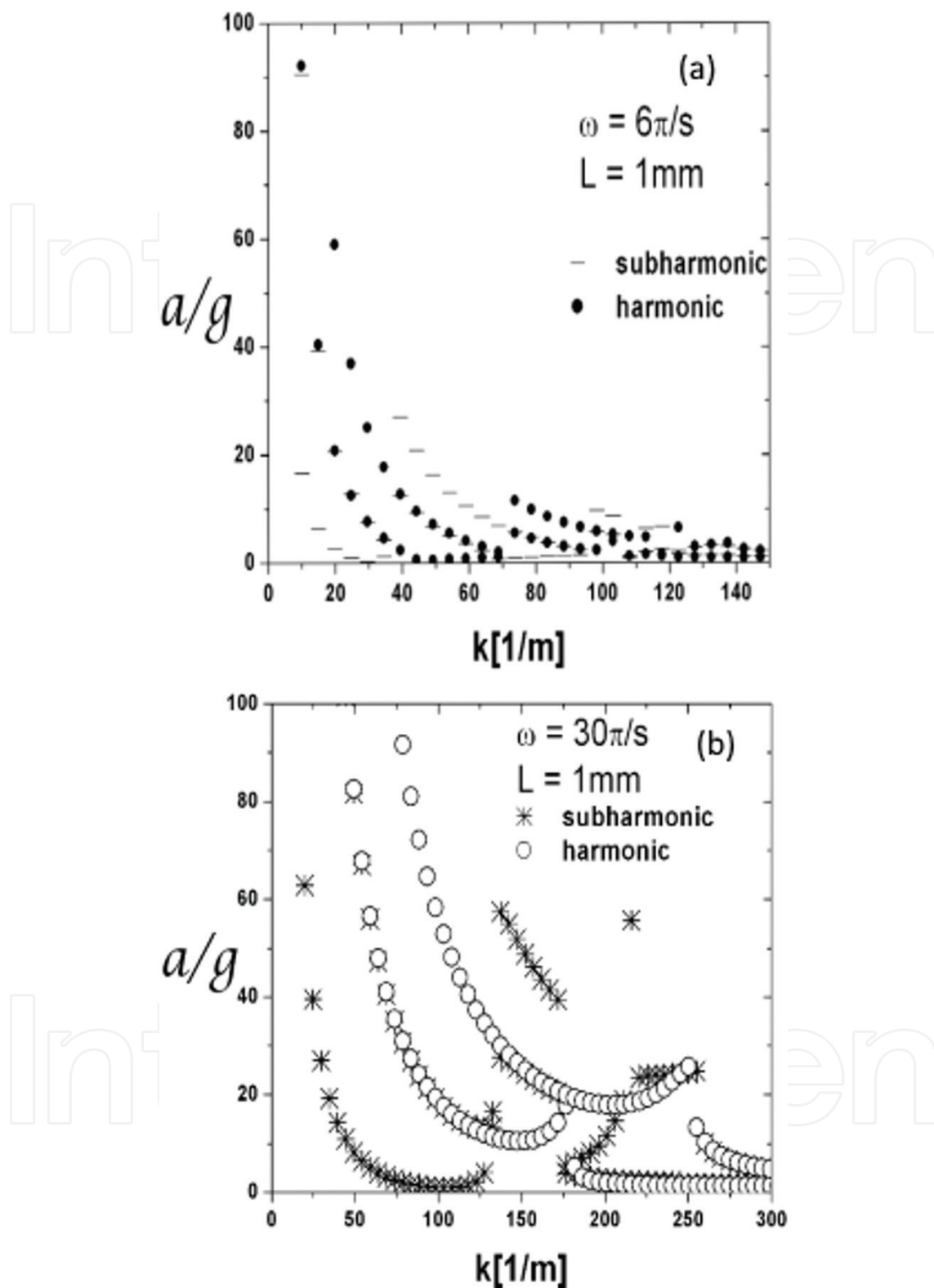
Figure 9. Plot of the acceleration versus wave number response of the surface wave sustained at the interface of a smectic A liquid-air for two frequencies and fixed room temperature. The configuration of the nematogens is given in **Figure 8**. The material parameters are provided in Section 3.1 and are typical of smectic A.
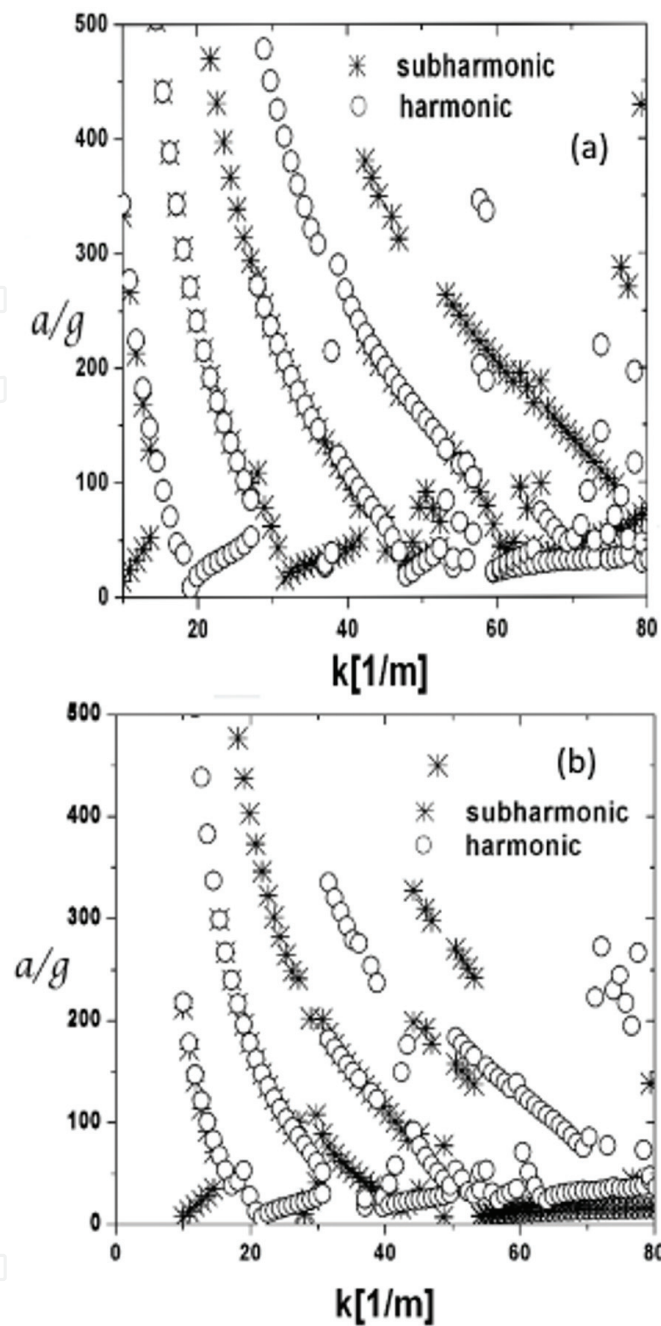
Figure 10. Neutral stability curve of Faraday wave at the interface of Sm A and air. There is no applied magnetic field. The nematogens are oriented in layers parallel to the interface and the flow velocity is in the *X*-axis direction. The material parameters used are given in the main text. Note that subharmonic waves are plotted with symbol *, whereas harmonic waves are depicted with ∘. This plot and that of **Figure 9** show that small depth Sm A liquid crystal layers can sustain parametric waves for excitation frequencies of typical experiments.

where the driving acceleration is plotted regarding the wave number. This picture shows us that parametric instability can be generated in shallow layers of smectic liquid crystals when it is excited with low frequencies. The magnitude of the normalized acceleration a/g falls well in the range of resolution of accessible experimental techniques that have been used before to

study other fluids. The material parameters used to make this plot correspond to typical smectic liquids: $K = 10^{-11}$ N, $B = 10^6$ N/m^2, $L = 10^{-4}$m, $\lambda_p = 10^{-14}$ m^4/Ns, $\rho = 10^3$ kg/m^3, $\eta_3 = 1$ P, $\eta_3 = \eta_2$, $\eta' = 10^{-2}\eta_3$, $\chi_a = 10^{-8}$ kg/(m s^2 G), $H = 3000$ G, the magnetic field that keeps fixed the orientation of nematogens, and $\gamma = 0.033$ N/m. In particular, **Figure 9a** points out that the excitation frequency $a/g \approx 0$ for the low frequency $\omega = 6\pi$ Hz, that is, infinitesimal accelerations, can excite subharmonic waves in a similar manner as it occurs in inviscid ideal fluids.

3.2. Smectic A layers parallel to the surface and no magnetic field

In this case, we derived the modes of the surface amplitude of deformation ζ_n that satisfies the eigenvalue Eqs. (27)–(29) with the function

$$M_n = \frac{2}{k}\left\{ w_0^2 + \left(\frac{Bk\sqrt{S_1}}{\rho} + \frac{\sqrt{S_1}}{k}\mu_n \left[\mu_n + k^2\left(3\nu_3 + \nu'\right) - \nu_3 S_1 \right] \right)\coth\left(L\sqrt{S_1}\right) \right\}. \qquad (31)$$

The curly brackets in the above expression for M_n with the value $n = 0$ yield the well now dispersion relationship of thermal capillary waves reported by other authors. In **Figure 10**, we depict the stability curve of external acceleration versus wave number at a fixed frequency of oscillation for the given material parameters; $K = 10^{-10}$ N, $B = 10^4$ N/m^2, layer thicknesses $L = 0.03$, 0.05 m, frequency $\omega = 18\pi$ Hz, $\lambda_p = 10^{-14}$ m^4/(N s), $\rho = 10^3$ kg/m^3, and viscosities and surface tension as in Section 3.1 earlier. We can observe that parametric surface waves also can evolve in this configuration of smectic A liquid. In a forthcoming manuscript, we will evaluate this parametric instability when the smectic phase can develop from the nematic phase as a thermal transition.

4. Lyotropic liquid crystal

In the previous section, we investigated how the bulk microstructure of the liquid crystal can modify the parametric instability through a thermal phase change. Now, we describe phase changes produced by particle volume fraction variations. Using birefringent measurements, Ballesta et al. [23] demonstrated a hydrodynamic phase change from isotropic to the nematic ordering of particles in a colloidal suspension. For the first time in the Faraday instability that occurs at the interface of air-colloidal suspension made of fd virus, they found that Faraday waves induce local nematic ordering of the nematogens in the wave crest when the colloid concentration is increased and close to the isotropic-nematic critical concentration. Such regions of nematic ordering become more permanent as the concentration is raised, and finally large areas of stable nematic patches that follow the wave flow are developed. This phenomenon was interpreted as a change in the local viscosity from its unperturbed value and decreases as a function of shear generated by the surface movement, which may reach high values of 100 Hz. A consequence of such shear thinning of viscosity is the appearance of hysteresis in the amplitude of the normal direction of the surface deformation as a function of the driving acceleration. Their analysis of the hysteretic behavior of the wave amplitude required them to use the Cross model of viscosity for bulk Newtonian fluids. Whereas for interpreting the intensity of observed birefringent experiments, it was necessary to use the

viscosity, and order parameter of a model of rod-like suspension of particles in the isotropic phase [60]. A recent complete numerical simulation of the hydrodynamic equations governing the Faraday waves was developed by Perinet et al. [61] for a system formed by two immiscible fluids with the supporting fluid forming a shallow layer smaller than its boundary layer. These authors confirmed a hysteresis of the amplitude of the surface deformation as a function of the driving acceleration. They conclude that the wave amplitude bifurcates into two different waves. The hysteresis of the lower amplitude wave is attributed to a change of the shear stress in the fluid that results from variations in the fluid flow that produce a balance of hydrostatic and lubrication stresses.

Unlike lyotropic liquids, a successful continuum mean field model for thermotropic nematics has allowed the description of the rheology of the bulk of confined layers of nematics under oscillatory shear. Such a model has predicted shear thinning of the viscosity as a function of the oscillation frequency of the imposed shear. The extension of this study to understand the shear thinning effect on viscosity in the experiments of Ref. [23] seems feasible. A different perspective is obtained with computer simulations as those made by Germano et al. [38]. These researches have shown through molecular dynamics simulations on a molecular model of bulk ellipsoids with pair interaction of Weeks-Chandler-Andersen type as they say "nematic fluids may adopt inhomogeneous steady states under shear flow" [38]. Thus, shear flow modifies the molecular ordering in the liquid crystal producing changes in macroscopic viscosities like shear thinning and thickening and shear banding similarly as that found by Ballesta in their experiment of fd virus suspension under parametric instability. However, those simulations cannot be compared directly with the experiments of Ballesta [23]. Germano et al. [38] were interested in the capillary waves spectrum at the interface formed during the transition from nematic to isotropic. However, they did compare their simulations with a theory of Landau-De Gennes type for the free energy of the interface which incorporates an average director parallel to the interface. They found isotropic capillary waves that propagate at long wavelengths governed by the macroscopic surface tension. At short wavelength, however, the surface tension becomes anisotropic and depends on the wave vector. In a recent series of papers by Popa-Nita et al. [27–31], they developed a Landau-De Gennes theory to describe the capillary waves originating from thermal fluctuations, and at the interface of a ternary mixture of liquid crystal, colloid, and impurities. They considered both homeotropic (perpendicular to the interface) and also the variation of the nematic director. As in the Germano et al. method, Popa-Nita uses a free energy of the liquid crystal that predicts the bulk phase diagram, and additionally a Cahn-Hilliard equation was incorporated for taking into account the diffusion of impurities and colloids inside the liquid crystal. For such a mixture, they predicted the surface tension to decrease with the presence of colloids, whereas the impurities enhance its strength. Also, the temperature of the bulk phase transition is lowered on the pure liquid crystal nematic-isotropic transition temperature. The interfaces so formed experience thermal fluctuations. With the help of this approach, Popa-Nita were able to find that there are two regions of propagating capillary waves as it was also observed by Germano et al. in their simulation work. In the first region of long wavelengths, there is dissipation produced by shear flow and the ternary mixture behaves like an isotropic fluid which can be described by a single effective bulk viscosity. The hydrodynamic equations of the velocity field underlying that dispersion relation depends on the respective viscosity for each of the two phases formed which are

separated by a sharp interface. With appropriate boundary conditions on each thermodynamic phase, the dispersion relation of the capillary waves was predicted. The generated wave depends on the average effective constant surface tension of the nematic and isotropic interface. The propagating ripple depends on one viscosity and the compression and bending modulus of the surface. The second region corresponds to a diffuse gap of particles close to the interface and corresponds to low values of wavenumber. This wave is dominated by the relaxation of the order parameter and the surface tension which is dependent on the density variation within the diffuse zone and the inhomogeneous distribution of nematogens inside it. The boundary conditions consist of the matching of the velocity field inside the diffuse zone with that from the bulk isotropic and nematic regions. The theoretical model of Popa-Nita [27–31] might be useful to study Faraday waves in interfaces of phase-separated regions of liquid crystals as a function of the concentration of particles. Presently, the phase transition on bulk phases of liquid crystals constitutes a large body of knowledge [62], but its effect on the dynamical responses of parametric waves on the interfaces so formed in the transition is still an open subject of research.

5. Conclusion

We reviewed recent results underlying the hydrodynamics description of Faraday waves under a thermal phase transition in thermotropic nematic liquid crystals. The numerical evaluation of the effect of phase change on the critical acceleration at the onset of the instability points out its pertinent experimental observation with birefringence or surface light-scattering techniques. Consequently, other liquid crystals can be studied with this theoretical approach. In Section 4, one such experimental example of a lyotropic liquid crystal of fd virus was mentioned. Also, a correction to the conceptual framework of Sections 2 and 3 to include the effect of variations of volume fraction of particles that can lead to a phase transition can be considered in this case.

Acknowledgements

Author details

Martin Hernández Contreras

Address all correspondence to: marther@fis.cinvestev.mx

Physics Department, Center for Research and Advanced Studies of the National Polytechnic Institute, CD Mexico, Mexico

References

[1] Christiansen B, Alstrom P, Levinsen T. Ordered capillary-wave states: Quasicrystals, hexagons, and radial waves. Physical Review Letters. 1992;**68**:2157-2160. DOI: 10.1103/PhysRevLett.68.2157

[2] Edwards WS, Fauve S. Patterns and quasi-patterns in the Faraday experiment. Journal of Fluid Mechanics. 1994;**278**:123-148. DOI: 10.1017/S0022112094003642

[3] Kudrolli A, Pier P, Gollub JP. Superlattice patterns in surface waves. Physica D. 1998;**123**:99-111. DOI: 10.1016/S0167-2789(98)00115-8

[4] Arbell H, Fineberg J. Spatial and temporal dynamics of two interacting modes in parametrically driven surface waves. Physical Review Letters. 1998;**81**:4384-4387. DOI: 10.1103/PhysRevLett.81.4384

[5] Benjamin T, Ursell F. The stability of the plane free surface of a liquid in vertical periodic motion. Proceedings of the Royal Society A. 1954;**225**:505-501. DOI: 10.1098/rspa.1954.0218

[6] Kumar K, Tuckerman LS. Parametric instability of the interface of two fluids. Journal of Fluid Mechanics. 1994;**279**:49-68. DOI: 10.1017/S0022112094003812

[7] Benchhoefer J, Ego V, Manneville S, Johnson B. An experimental study of the onset of parametrically pumped surface waves in viscous fluids. Journal of Fluid Mechanics. 1995;**288**:325-350. DOI: 10.1017/S0022112095001169

[8] Müller HW, Zimmermann W. Faraday instability in a linear viscoelastic fluid. Europhysics Letters. 1999;**83**:169-174. DOI: 10.1209/epl/i1999-00142-5

[9] Wagner C, Müller HW, Knorr K. Faraday waves on a viscoelastic liquid. Physical Review Letters. 1999;**83**:308-311. DOI: 10.1103/PhysRevLett.83.308

[10] Kumar S. Vibration-induced interfacial instabilities in viscoelastic fluids. Physical Review E. 2002;**65**:026305. DOI: 10.1103/PhysRevE.65.026305

[11] Kumar S, Fauve S. Faraday instability with a polymer solution. The European Physical Journal B. 1999;**9**:175-178. DOI: 10.1007/s100510050753

[12] Kumar S. Parametrically driven surface waves in viscoelastic liquids. Physics of Fluids. 1999;**11**:1970-1981. DOI: 10.1063/1.870061

[13] Ovando-Vazquez C, Vazquez Rodriguez O, Hernandez-Contreras M. Faraday waves on finite thickness smectic a liquid crystal and polymer gel materials. AIP Conference Proceedings. 2008;**1077**:135-141. DOI: 10.1063/1.3040251

[14] Ballesta P, Manneville S. Signature of elasticity in the Faraday instability. Physical Review E. 2005;**71**:026308. DOI: 10.1103/PhysRevE.71.026308

[15] Müller HW. Parametrically driven surface waves on viscous ferrofluids. Physical Review E. 1998;**58**:6199-6205. DOI: 10.1103/PhysRevE.58.6199

[16] Mekhonoshin VV, Lange A. Faraday instability on viscous ferrofluids in a horizontal magnetic field: Oblique rolls of arbitrary orientation. Physical Review E. 2002;**65**:061509. DOI: 10.1103/PhysRevE.65.061509

[17] Perinet N, Juric D, Tuckerman LS. Numerical simulation of Faraday waves. Journal of Fluid Mechanics. 2009;**635**:1-26. DOI: 10.1017/S0022112009007551

[18] Kityk AV, Embs J, Mekhonoshin VV, Wagner C. Spatiotemporal characterization of inter-facial Faraday waves by means of a light absorption technique. Physical Review E. 2005;**72**:036209. DOI: 10.1103/PhysRevE.72.036209

[19] Zhang W, Viñals J. Pattern formation in weakly damped Faraday waves. Journal of Fluid Mechanics. 1997;**336**:301-330. DOI: 10.1017/S0022112096004764

[20] Chen P, Viñals J. Amplitude equation and pattern selection in Faraday waves. Physical Review E. 1999;**60**:559-570. DOI: 10.1103/PhysRevE.60.559

[21] Skeldon AC, Guidoboni G. Pattern selection for Faraday waves in an incompressible viscous fluid. SIAM Journal on Applied Mathematics. 2007;**67**:1064-1100. DOI: 10.1137/050639223

[22] Silber M, Topaz C, Skeldon AC. Two-frequency forced Faraday waves: Weakly damped modes and pattern selection. Physica D. 2000;**143**:205-225. DOI: 10.1016/S0167-2789(00)00102-0

[23] Ballesta P, Lettingaa MP, Manneville S. Interplay between a hydrodynamic instability and a phase transition: The Faraday instability in dispersions of rodlike colloids. Soft Matter. 2011;**7**:11440-11446. DOI: 10.1039/c1sm06175e

[24] Epstein T, Deegan RD. Strip waves in vibrated shear-thickening wormlike micellar solu-tions. Physical Review E. 2010;**81**:066310. DOI: 10.1103/PhysRevE.81.066310

[25] Price AD, Schwartz DK. Fatty-acid monolayers at the nematic/water interface: Phases and liquid-crystal. Journal of Physical Chemistry B. 2007;**111**:1007-1015. DOI: 10.1021/jp066228b

[26] Clare BH, Abbott NL. Orientations of nematic liquid crystals on surfaces presenting controlled densities of peptides: Amplification of protein−peptide binding events. Lang-muir. 2005;**21**:6451-6461. DOI: 10.1021/la050336s

[27] Popa-Nita V, Oswald P. Surface tension and capillary waves at the nematic-isotropic interface in ternary mixtures of liquid crystal, colloids, and impurities. Journal of Chem-ical Physics. 2007;**127**:104702. DOI: 10.1063/1.2772251

[28] Popa-Nita V, Sluckin TJ, Kralj S. Waves at the nematic-isotropic interface: Thermotropic nematogen–non-nematogen mixtures. Physical Review E. 2005;**71**:061706. DOI: 10.1103/PhysRevE.71.061706

[29] Popa-Nita V, Sluckin TJ. Surface modes at the nematic-isotropic interface. Physical Review E. 2002;**66**:041703. DOI: 0.1103/PhysRevE.66.041703

[30] Popa-Nita V, Oswald P. Waves at the nematic-isotropic interface: The role of surface tension anisotropy, curvature elasticity, and backflow effects. Physical Review E. 2003;**68**:061707. DOI: 10.1103/PhysRevE.68.061707

[31] Popa-Nita V, Oswald P, Sluckin TJ. Waves at the nematic-isotropic interface. Molecular Crystals and Liquid Crystals. 2005;**435**:215/[875]-232/[892]. DOI: 10.1080/15421400590955299

[32] Lishchuk SV. Waves at surfactant-laden liquid-liquid crystal interface. Physical Review E. 2007;**76**:011711. DOI: 10.1103/PhysRevE.76.011711

[33] Lishchuk SV. Scattering of light on surfactant-laden liquid-liquid crystal interface. Chemical Engineering Communications. 2009;**196**:854-871. DOI: 10.1080/00986440802668174

[34] Rey AD. Viscoelastic theory for nematic interfaces. Physical Review E. 2000;**61**:1540. DOI: 10.1103/PhysRevE.61.1540

[35] Rey AD. Mechanical model for anisotropic curved interfaces with applications to surfactant-laden liquid-liquid crystal interfaces. Langmuir. 2006;**22**:219-228. DOI: 10.1021/la051974d

[36] Rey AD. Polar fluid model of viscoelastic membranes and interfaces. Journal of Colloid and Interface Science. 2006;**304**:226-238. DOI: 10.1016/j.jcis.2006.08.027

[37] Schmid F, Germano G, Wolfsheimer S, Chilling T. Fluctuating interfaces in liquid crystals. Macromolecular Symposia. 2007;**252**:110-118. DOI: 10.1002/masy.200750611

[38] Germano G, Schmid F. Nematic-isotropic interfaces under shear: A molecular-dynamics simulation. Journal of Chemical Physics. 2005;**123**:214703. DOI: 10.1063/1.2131065

[39] Hernández-Contreras M. Faraday waves on nematic liquid crystals: Effect of Marangoni flow and thermal phase transition. Physical Review E. 2013;**88**:062311

[40] Hernández-Contreras M. Faraday waves in smectic A liquid crystal layers. Journal of Physics: Condensed Matter. 2010;**22**:035106. DOI: 10.1088/0953-8984/22/3/035106

[41] Lockwood NA, Abbott NL. SSelf-assembly of surfactants and phospholipids at interfaces between aqueous phases and thermotropic liquid crystals. Current Opinion in Colloid & Intface Science. 2005;**10**:111-120. DOI: 10.1016/j.cocis.2005.06.002

[42] Lockwood N.A, Gupta J.K, Abbot N.L. Self-assembly of amphiphiles, polymers and proteins at interfaces between thermotropic liquid crystals and aqueous phases. Surface Science Reports. 2008;**63**:255-293. DOI: 10.1016/j.surfrep.2008.02.002

[43] Crawford GP, Ondris-Crawford RJ, Doane JW, Žumer S. Systematic study of orientational wetting and anchoring at a liquid-crystal-surfactant interface. Physical Review E. 1996;**53**:3647. DOI: 10.1103/PhysRevE.53.3647

[44] Fazio VSU, Nannelli F, Komitov L. Sensitive methods for estimating the anchoring strength of nematic liquid crystals. Physical Review E. 2001;**63**:061712. DOI: 10.1103/PhysRevE.63.061712

[45] Bahr C. Surfactant-induced nematic wetting layer at a thermotropic liquid crystal/water interface. Physical Review E. 2006;**73**:030702. DOI: 10.1103/PhysRevE.73.030702

[46] Poulin P, Stark H, Lubensky TC, Weitz DA. Novel colloidal interactions in anisotropic fluids. Science. 1997;**275**:1770-1773. DOI: 10.1126/science.275.5307.1770

[47] Figuereido Neto A, SRA S, editors. The Physics of Lyotropic Liquid Crystals: Phase Transitions and Structural Properties. 1st ed. New York: Oxford University Press; 2005. p. 301. DOI: 10.0198525508

[48] Langevin D. Spectre des fluctuations thermiques à la surface libre d'un cristal liquide smectique A en présence d'un champ magnétique horizontal. Journal de Physique France. 1976;**37**:737-746. DOI: 10.1051/jphys:01976003706073700

[49] Buzza DMA, Jones JL, McLeish TCB, Richards RW. Theory of surface light scattering from a fluid–fluid interface with adsorbed polymeric surfactants. Journal of Chemical Physics. 1998;**109**:5008-5024. DOI: 10.1063/1.477114

[50] Crilly JF, Earnshaw JC. A light scattering study of thermotropic transitions of monoglyceride monolayers: Influence of molecular area fluctuations. Journal de Physique France. 1987;**48**:485-494. DOI: 10.1051/jphys:01987004803048500

[51] Langevin D. Analyse spectrale de la lumière diffusée par la surface libre d'un cristal liquide nématique. Mesure de la tension superficielle et des coefficients de viscosité. Journal de Physique France. 1972;**33**:249-256. DOI: 10.1051/jphys:01972003302-3024900

[52] Hernández-Contreras M, Kim MW, Pincus P. Surface hydrodynamics on a freely standing layer of a polymer solution. Physical Review E. 1999;**60**:4319-4329. DOI: 10.1103/PhysRevE.60.4319

[53] Langevin D. Light-scattering study of monolayer viscoelasticity. Journal of Colloid & Interface. Science. 1981;**80**:412-425. DOI: 10.1016/0021-9797(81)90200-9

[54] Langevin D, editor. Light Scattering by Liquid Surfaces and Complementary Techniques. 1st ed. New York: Marcel Dekker; 1992. p. 472. DOI: 10.0824786076

[55] Earnshaw JC. Light scattering studies of interfacial rheology. Journal of Dispersion Science and Technology. 1999;**20**:743-765. DOI: 10.1080/019322699908943818

[56] Giermanska-Khan J, Monroy F, Langevin D. Negative effective surface viscosities in insoluble fatty acid monolayers: Effect of phase transitions on dilational viscoelasticity. Physical Review E. 1999;**60**:7163-7173. DOI: 10.1103/PhysRevE.60.7163

[57] Huber P, Soprunyuk VP, Embs JP, Deutsch WCM. Faraday instability in a surface-frozen liquid. Physical Review Letters. 2005;**94**:184504. DOI: 10.1103/PhysRevLett.94.184504

[58] Langevin D, Bouchiat MA. Spectre des fluctuations thermiques a la surface libre d'un cristal liquide nématique. Journal de Physique France. 1972;**33**:101-111. DOI: 10.1051/jphys:01972003301010100

[59] Urbach W, Hervet H, Rondelez F. Thermal diffusivity measurements in nematic and smectic phases by forced Rayleigh light scattering. Molecular Crystals and Liquid Crystals. 1978;**46**:209-221. DOI: 10.1080/00268947808083724

[60] Dhont JKG, Briels WJ. Viscoelasticity of suspensions of long, rigid rods. Colloids and Surfaces A. 2003;**213**:131-156. DOI: 10.1016/S0927-7757(02)00508-3

[61] Périnet N, Falcón C, Chergui J, Juric D, Shin S. Hysteretic Faraday waves. Physical Review E. 2016;**93**:063114. DOI: 10.1103/PhysRevE.93.063114

[62] Singh S. Phase transitions in liquid crystals. Physics Reports. 2000;**324**:107-269. DOI: 10.1016/S0370-1573(99)00049-6